Dynamics of evaporative cooling for Bose-Einstein condensation

Huang Wu,[1] Ennio Arimondo,[1] and Christopher J. Foot[2]
[1]*Unità Istituto Nazionale di Fisica della Materia, Dipartimento di Fisica, Università di Pisa, 56126 Pisa, Italy*
[2]*Clarendon Laboratory, Parks Road, Oxford OX1 3PU, United Kingdom*
(Received 21 November 1996)

We have simulated the evaporative cooling of a dilute gas of Bose particles including quantum statistics using a Monte Carlo method. This approach can model situations which are far away from quasiequilibrium such as occur during forced evaporative cooling. We have also simulated the dynamical formation of Bose-Einstein condensate for homogeneous and inhomogeneous Bose gases under the random-phase approximation. It was found that the rate of accumulation of Bose particles into low-energy states through collisions is increased by forced evaporation; and a macroscopic population at ground state can be reached at a time scale characterized by classical collision time for an inhomogeneous gas in a harmonic potential. We present the results of simulations for the evaporative cooling and formation of a Bose-Einstein condensate in one-, two-, and three-dimensional position cuts and energy cuts. [S1050-2947(97)04506-X]

PACS number(s): 03.75.Fi, 32.80.Pj, 67.65.+z

I. INTRODUCTION

The technique of evaporative cooling of magnetically trapped atoms was first applied to atomic hydrogen [1,2] and recently it has been used very successfully on alkali-metal atoms [3,4] leading to Bose-Einstein condensation [5–7]. It relies on the escape from an isolated system, such as a magnetic trap, of a small portion of atoms having the largest energy, and on the rethermalization of the remaining atoms to a lower temperature. When this process is repeated continuously by, for example, progressively reducing the potential barrier confining the atoms, it is possible to bring the remaining atoms to a very low temperature. This schematic description of the evaporative cooling process shows that it is necessary to have short interatomic collision times in order to produce a rapid thermalization of the atoms in the trap.

Theoretical models of evaporative cooling are useful in understanding experiments and optimizing them to give efficient cooling and a large final number of atoms. So far there have been four methods developed to study evaporative cooling [8–12]. Except for the Bird method introduced in Ref. [11] and used in this paper, the other three consider energy evolution and use the assumption of sufficient ergodicity [13] for simplifying the description of a gas in a trap. The use of the classical Monte Carlo method developed by Bird for gas dynamics enables a direct Monte Carlo simulation to be carried out, which gives the position and velocity of each atom at each time step, without the need to keep close to quasiequilibrium distributions for velocity or position. Bird's method was developed through consideration of the physics of the way a gas flows, that is, the motion of atoms and collisions between them [14]. This Monte Carlo method gives an accurate representation in the molecular flow regime and is consistent with the Boltzmann equation. Furthermore, since Bird's method does not rely on the assumption of inverse collisions (the same cross section for the time-reversed situation), it can be applied to describe complex phenomena such as associative ionization, dissociation, and trap loss, which are inaccessible to the Boltzmann formulation.

In this paper we present the results of direct simulation of population dynamics of homogeneous and inhomogeneous gases by using the Bird method. In the simulation of evaporative cooling presented here we have considered Bose statistics, while all the simulations published before were purely classical [8–11]. Our numerical analysis is performed with parameters corresponding to those of Refs. [5,6] for alkali-metal systems, and our simulations give the values of the fraction of atoms remaining after evaporative cooling, their temperature, and the fraction of atoms in the ground state. Using these simulations we study the efficiency of the evaporative cooling for different evaporation procedures, e.g., cuts in energy or position.

In our analysis we have concentrated on the time scale for the rethermalization and the evaporative cooling processes. Depending on the interatomic collision rate, the speed of ramping down the trap depth in forced evaporation, and the geometric structure of a trap [11,13], the distribution of atoms in phase space may deviate significantly from thermal equilibrium.

As an important feature, the Bird method does not require the assumption of sufficient ergodicity, as in most previous analysis of evaporative cooling. Sufficient ergodicity assumes that the distribution of atoms in phase space depends only on their energy. This will be the case in a trap with single-particle motion, in which case all parts of the equipotential hypersurface corresponding to the total energy of the atom are sampled with equal probability [13]. If the ergodic mixing time is longer than the elastic collision time, the ergodicity assumption is not valid, because the atomic energies along different directions are separable and cannot be described by a single temperature [11,12]. If evaporative cooling is operated in these conditions the removing of hot atoms becomes based on the selection of energy along some particular directions instead of their total energy [12]. It could be stated that due to the difference between different directions in kinetic or potential energies or their sum, evaporative cooling in one or two dimensions formally cannot lead to an ergodic system [11]. Even if the most recent evaporative cooling experiments of alkali-metal atoms were sup-

posed to have operated in conditions of sufficient ergodicity, the conditions should be tested more carefully in the future. In any case, a nonergodic situation has been realized in several atomic traps [4,15,16], where ergodic mixing of many seconds was observed, much longer than typical elastic collision times of milliseconds to a second [12]. As a result of our numerical simulations in a previous work [11], a difference in atomic temperature (mean energy) between different directions was observed, directly proving that a nonergodic system may be created by evaporative cooling. In the present work, we derive an atomic distribution which cannot be fitted within the frame of the ergodicity assumption, and the results point out that our approach produces a better description of the evaporative cooling process.

Section II presents the simulation method and discusses how the quantum statistics effects of the Bose atoms are included into the simulation process. Section III describes the results of our simulations: the evaporative cooling of sodium atoms is investigated for efficiency in final temperature, and remaining fraction of atoms following different evaporation processes and varying the rates of evaporative cooling. The last part of Sec. III presents a comparison with a previous analysis of evaporative cooling.

II. THE BASIS OF THE THEORY

A. The simulation method

The basic principle of the Bird method has been described elsewhere [11,14]. Here we give a brief description of this distinguished method, which is a well-known technique in molecular gas dynamics. Bird's method was developed through consideration of the physics of gas flow, i.e., the motion of atoms and collisions between them [11,14], which is in contrast with the mathematical description of the Boltzmann equation [9,17]. It has been proven that the Bird method gives an accurate representation in the molecular flow regime and that it is consistent with the Boltzmann equation in phase space [14]. This very powerful method is widely applied in many areas, such as nonequilibrium flow of gas [18,19], evaporation and condensation for plasma-facing materials in fusion reaction [20,21], wake effects in aerospace [22], vacuum deposition [23], Rayleigh-Bénard convection [24], and expansion cooling of vapors [25–27].

The microscopic model of gas recognizes the particular structure of the gas as a myriad of discrete atoms or molecules and ideally provides information on the position and velocity of every atom at all times when internal degrees of freedom are neglected. For a real gas, once an atom's initial momentum and position are specified, it is sufficient to determine completely its future information, if it were not for the interaction with other atoms. Although collisions are rare in the region of interest where mean free path λ is much larger than the characteristic dimension L, or the Knudsen number $K_n=\lambda/L$ is much larger than one (we note that, in fact, the mean free path is comparable to the trap dimension by the end of evaporation in Ref. [6,38]), they are frequent enough to make the accurate simulation of the trajectories of an individual atom a quite impractical task. The intermolecular collisions not only result in the difficulty of direct simulation of gas flow, but also make the direct solution of the Boltzmann equation in six-dimensional phase space to be nearly impossible. However, the discrete structure of the gas at the molecular gas level enables these difficulties to be circumvented through direct physical modeling when one essential feature of Bird's method is applied: allowing the molecular motion and the intermolecular collisions to be uncoupled over a small time interval Δt_m. It has been proved that so long as Δt_m is much less than the mean collision time Δt_c, this model can give a very accurate description of gas flow [14]. For this physical model the calculation time is linearly proportional to the number of atoms in the simulation and it is numerically stable—methods involving the nonlinear Boltzmann equation do not share these characteristics. In this model, the simulated position space is divided into many cells within which atoms are randomly located. These cells are an array of points. An atom is said to be in a cell when it is nearest to the point which specifies that cell. The point reference scheme avoids the necessity of providing an analytical description of the cell boundaries and provides more continuous distribution of atoms in position space. The dimensions $\Delta\mathbf{r}$ of the cells must be such that the change in vapor properties across each cell must be small. Time is advanced in discrete steps of magnitude Δt_m, which are small compared with mean collision time and ensure the distance through which an atom moves in a given time step and is not large compared to the changes in the potential. In our calculation, the time step was chosen to be between $0.05\Delta t_c$ to $0.0002\Delta t_c$. The calculation proceeds as follows. In the first step all the atoms are moved through distances appropriate to their velocity components $\mathbf{V}_n$ and Δt_m: $\mathbf{r}_{n+1}=\mathbf{r}_n+\mathbf{V}_n\Delta t_m$. Appropriate action is taken if the atom crosses boundaries representing the edge of the potential, i.e., it is reflected or lost. The second step is to compute the effect of collisions among the atoms in each cell during Δt_m. The interatomic collisions are assumed to be binary and instantaneous. They are treated consistently with classical collision dynamics, i.e., the conservation of momentum and energy is strictly obeyed and the uncertainty principle is not considered. The choice of the pairs of atoms in a cell which might collide is made randomly: but whether or not they do actually collide is determined using an acceptance-rejection method [28]—the probability of the collision being proportional to their relative velocity as usual in kinetic theory. By this procedure the calculation time is proportional to the number of atoms instead of its square [14]. The precollision velocity components of the pair of colliding atoms are replaced by the postcollision values. Thus a collision is simply equivalent to a jump in velocity space, while the positions of the colliding atoms remain unchanged. The collision dynamics is dealt with in the center of mass frame and the resultant velocity is obtained by transforming back to the laboratory coordinate system. When the scattering is isotropic, two scattering angles, $\phi=2\pi R_{\text{random}}(0,1)$ and $\cos\theta=(1-2)\times R_{\text{random}}(0,1)$, are used to parametrize the scattering process. The random number R_{random} is uniformly selected between 0 and 1. The hard-sphere model is used since in evaporative cooling the s-wave elastic scattering is dominant, although a variable hard-sphere model and variable soft model can be implemented in this method [14]. The third stage is to consider the change of the velocity components of atoms, of mass M, resulting from the gradient of the potential $U(\mathbf{r})$

$$\Delta \mathbf{v}_n = \frac{-\nabla U(\mathbf{r})}{M} \Delta t_m . \tag{1}$$

In this paper we consider a three-dimensional harmonic potential to describe the magnetic trap where evaporative cooling of alkali-metal cold atoms has been performed

$$U(\mathbf{r}) = \tfrac{1}{2} M(\omega_x^2 \mathbf{x}^2 + \omega_y^2 \mathbf{y}^2 + \omega_z^2 \mathbf{z}^2), \tag{2}$$

here ω_i is the angular oscillation frequency of atoms in the potential.

As the final part of the description of this method, we discuss the effects of the statistical fluctuations and random walk that are inevitable in all results from the Monte Carlo method. A cell of volume V contains a number N of atoms and this number is subject to statistical fluctuation about the mean value nV, where n is the mean density. The probability $P(N)$ of a particular value of N is given by the Poisson distribution

$$P(N) = (nV)^N \exp(-nV)/N! \tag{3}$$

For large values of nV, this distribution becomes indistinguishable from a Gaussian distribution

$$P(N) \simeq (2\pi nV)^{-1/2} \exp[-(N-nV)^2/(2nV)]. \tag{4}$$

For this distribution the standard deviation for the fluctuation of N from its mean value is $1/\sqrt{nV}$, and for low N values this fluctuation could be relevant. Random walks can arise whenever one of the atomic quantities is conserved only on the average, rather than exactly, in any of the simulation procedures. The atomic quantities of interest are the position coordinates and the velocity components. Random walks arise because the position and velocity are rounded off in order to be stored as a discrete value rather than as an exact number at the final stage of simulation when results are output. The effect of random walks also appears in quantum Monte Carlo simulation [29]. Due to the limited precision with which variables are manipulated, some degree of rounding is unavoidable. This effect was investigated in the present simulation by monitoring the total energy in a direct simulation with a fixed sample of 10 000 atoms in a harmonic potential and in a homogeneous gas. After each atom experienced 100 collisions in average, the total energy was found to fluctuate by no more than one part in a hundred. This shows that the error caused by random walks is of acceptable magnitude [11].

B. Collision rate

The collision rate, whose increase results in run-away evaporation, is an important parameter in evaporative cooling. It is especially important to calculate the collision rate correctly since in our calculations time is expressed in units of initial collision times and, therefore, one needs to know what this is in order to compare it with reality. In thermal equilibrium the phase-space distribution $f(\mathbf{r},\mathbf{p})$ of a classical ideal gas in a potential field $U(\mathbf{r})$ is described by

$$f(\mathbf{r},\mathbf{p}) = n_0 (2\pi M k_B T)^{-3/2} e^{[-(U(\mathbf{r}) + p^2/2M)/k_B T]}, \tag{5}$$

where k_B is the Boltzmann constant and p is the magnitude of atomic momentum $\mathbf{p}$. The central density n_0 is chosen in such a way that the phase-space distribution function $f(\mathbf{r},\mathbf{p})$ is normalized to the total particle number $N = \int d^3r d^3p f(\mathbf{r},\mathbf{p})$, where the integration is over the available phase space. By integrating over the whole momentum space we obtain the spatial density distribution

$$n(\mathbf{r}) = n_0 e^{-U(\mathbf{r})/k_B T}. \tag{6}$$

For any thermal distribution we may write the collision event rate as [13,30]

$$\Gamma_c = \frac{1}{2M} \int d^3r \int d^3p_1 \int |\mathbf{p}_2 - \mathbf{p}_1| \sigma f(\mathbf{r},\mathbf{p_1}) f(\mathbf{r},\mathbf{p_2}) d^3p_2 . \tag{7}$$

When the elastic hard-sphere model is used, the collision cross section σ will be independent of the relative momentum $\mathbf{p_r} = \mathbf{p_2} - \mathbf{p_1}$ and position $\mathbf{r}$. In evaporative cooling, atoms with energy larger than potential barrier U_m escape from the trap and a truncated distribution is obtained because the integration is over all $(\mathbf{r},\mathbf{p})$, for which

$$U(\mathbf{r}) + p_{1,2}^2/2M \leqslant U_m . \tag{8}$$

Thus the integration boundaries of $\mathbf{r}$ and $\mathbf{p}$ are coupled together through Eq. (8). So the evaluation of Γ_c involves a complicated nested triple integral. When we start with a near stationary Maxwell-Boltzmann distribution as the initial distribution (the cut energy of the potential is much larger than the mean energy of the atomic cloud), the boundaries of $\mathbf{r}$ and $\mathbf{p}$ can be set to infinity. Then the calculation of the initial collision rate is much simpler. Bringing Eq. (5) into Eq. (7), using the center-of-mass frame and reexpressing the resulting equation in terms of velocities for convenience, $\mathbf{v_m} = (\mathbf{v_2} + \mathbf{v_1})/2, \mathbf{v_r} = (\mathbf{v_2} - \mathbf{v_1})$, we find

$$\begin{aligned}
\Gamma_c &= \frac{\sigma M^3}{2(2\pi k_B T)^3} \int n_0^2 e^{-2U(\mathbf{r})/k_B T} d^3r \\
&\quad \times \int e^{-M v_m^2/k_B T} d^3v_m \int v_r e^{-M v_r^2/4k_B T} d^3v_r \\
&= \frac{\sigma N M^3 \overline{n(\mathbf{r})}}{2(2\pi k_B T)^3} \int d^3v_m e^{-M v_m^2/k_B T} \int d^3v_r v_r e^{-M v_r^2/4k_B T} \\
&= \frac{1}{\sqrt{2}} N \overline{n(\mathbf{r})} \sigma \overline{v},
\end{aligned} \tag{9}$$

where the mean density is defined as

$$\overline{n(\mathbf{r})} = \frac{\int n_0^2 e^{-2U(\mathbf{r})/k_B T} d^3r}{N} = \frac{\int n^2(\mathbf{r}) d^3r}{\int n(\mathbf{r}) d^3r} \tag{10}$$

and $\overline{v} = \sqrt{8k_B T/\pi M}$. The mean collision rate for each atom is then

$$\overline{\nu} = \frac{2\Gamma_c}{N} = \sqrt{2}\, \overline{n(\mathbf{r})} \sigma \overline{v}, \tag{11}$$

where the factor 2 indicates each collision involving two atoms. It is important to note that Eq. (11) can be applied to homogeneous and inhomogeneous gases. The initial collision time τ_i, which is used as time unit in the following sections, is defined as the inverse of the initial mean collision rate:

$$\tau_i = 1/\overline{\nu_i}. \tag{12}$$

For a thermal equilibrium gas in a harmonic potential, the central density is

$$n_0 = N\omega_x\omega_y\omega_z\left(\frac{M}{2\pi k_B T}\right)^{3/2}. \tag{13}$$

The mean density is

$$\overline{n(\mathbf{r})} = N\omega_x\omega_y\omega_z\left(\frac{M}{4\pi k_B T}\right)^{3/2}. \tag{14}$$

Hence,

$$n_0/\overline{n(\mathbf{r})} = \sqrt{8}. \tag{15}$$

The mean collision rate of the cloud can be obtained in an alternative way, starting from the local collision rate

$$\nu(\mathbf{r}) = n(\mathbf{r})\sigma v_r, \tag{16}$$

where $\mathbf{v_r}=\mathbf{v_2}-\mathbf{v_1}$. The mean collision rate is obtained by summing over all velocity classes and therefore over all values of v_r, i.e.,

$$\overline{\nu} = \overline{n(\mathbf{r})}\sigma\overline{v_r}. \tag{17}$$

Because the hard-sphere model is used, σ is a constant (i.e., independent of v_r). The separation, $\overline{n(\mathbf{r})v_r} = \overline{n(\mathbf{r})}\,\overline{v_r}$ only holds when the limits of the position and velocity (momentum) integrals are infinity. The average value $\overline{n(\mathbf{r})}$ is obtained from the definition

$$\overline{n(\mathbf{r})} = \frac{\int_{-\infty}^{\infty} n^2(\mathbf{r})\,dx\,dy\,dz}{\int_{-\infty}^{\infty} n(\mathbf{r})\,dx\,dy\,dz}. \tag{18}$$

This is the form used in the computations and is obviously equivalent to Eq. (10) where $n(\mathbf{r})$ is Gaussian. The average value of $\overline{v_r}$ is obtained from the following expression:

$$\overline{v_r} = \int\int_{-\infty}^{\infty} v_r f(\mathbf{v}_1) f(\mathbf{v}_2)\,d\mathbf{v_1}\,d\mathbf{v_2}, \tag{19}$$

which, for Maxwellian velocity distribution $f(\mathbf{v}_1)$ and $f(\mathbf{v}_2)$, gives the well-known kinetic theory result $\overline{v_r} = \sqrt{2}\,\overline{v_a}$. Hence, this method gives Eq. (11).

C. Scattering of two Bose particles

The dynamical formation of the Bose-Einstein condensate can be classified into three stages: kinetic evolution, the formation of short-range order and the off-diagonal long-range order [32–34]. The time scale for the first stage is characterized by interatomic collision time and is much longer than the second stage and can be comparable to the third stage. So the kinetic evolution basically determines the time scale for the formation of the Bose-Einstein condensate. During the first stage, Bose particles are pushed by scattering into the energy regimes which are less than the interaction energy among particles. At this stage the random-phase approximation is valid but it breaks down when local-range order appears [31–35]. Under this approximation our model cannot study the appearance of coherence among Bose particles, but allows us to study the population dynamics of a condensate.

In terms of Bose statistics, the probability of two bosons with wave vectors $\mathbf{k_1},\mathbf{k_2}$ scattering into $\mathbf{k_3},\mathbf{k_4}$ is [31,32],

$$S(\mathbf{k_1},\mathbf{k_2};\mathbf{k_3},\mathbf{k_4}) = T_m^2\,\delta(\mathbf{k_1}+\mathbf{k_2}-\mathbf{k_3}-\mathbf{k_4})\,\delta(E_1+E_2-E_3-E_4) \times f(\mathbf{k_1})f(\mathbf{k_2})[1+f(\mathbf{k_3})][1+f(\mathbf{k_4})], \tag{20}$$

where T_m is the matrix element of the interaction, and $T_m^2 f(\mathbf{k_1})f(\mathbf{k_2})$ shows the classical rate where the effects of quantum statistics can be ignored. The most important factors in Eq. (20) are $[1+f(\mathbf{k_3})]$ and $[1+f(\mathbf{k_4})]$, which means that in a collision for Bosons, the scattering probability into a state which already contains $f(\mathbf{k_i})$ Bose particles is $1+f(\mathbf{k_i})$ times stronger than it would be if there were no Bose particles present. This stimulated scattering process can be put into the simulation straightforwardly by using the acceptance and rejection method in Monte Carlo simulation [14,28]. That is to say that at each collision we make the probability distribution of the final velocities depend on the velocity distribution already existing *in that particular region of velocity space* in a way which takes into account the bosonic enhancement factors $[1+f(\mathbf{k_i})]$. It took around two hours to run a calculation of 20 initial collision times with $\sim 10^6$ atoms on a DEC alpha Server 2100 Open Vms AXP 6.1 machine.

III. SIMULATION RESULTS

A. A homogeneous gas

In order to make a comparison with inhomogeneous gas and also with a previous work [31], we first study a homogeneous gas consisting of $\sim 10^6$ sodium atoms. In fact, for inhomogeneous gases in an external potential, when the potential is balanced by the interaction energy among atoms, the properties of the gas should be similar to that of the homogeneous case. The initial density is 1.5×10^{14} cm^{-3}, and the initial temperature T_0 is $2\,\mu$K. For sodium atoms the chosen initial density corresponds to the critical one required for Bose-Einstein condensation at the temperature T_0 [6,38,12].

In Fig. 1(a) the full curve shows the particle energy distribution $n(E)$ after 80 scattering events. We note that even after experiencing more than 80 scattering events for each bosons (not shown), there is still a particle energy flux towards the low-energy regime, which indicates the equilibrium state has not yet been reached. This overall behavior is similar to that observed by Snoke and Wolfe [31]. It can be noted in Fig. 1(a) that the energy distribution is well fit by the Bose-Einstein distribution function $f(E,\mu,T)$, which is indicated by the dotted line,

$$f(E,\mu,T) = \frac{1}{e^{(E-\mu)/k_B T}-1} = \frac{1}{e^{(\epsilon+\alpha)}-1}, \tag{21}$$

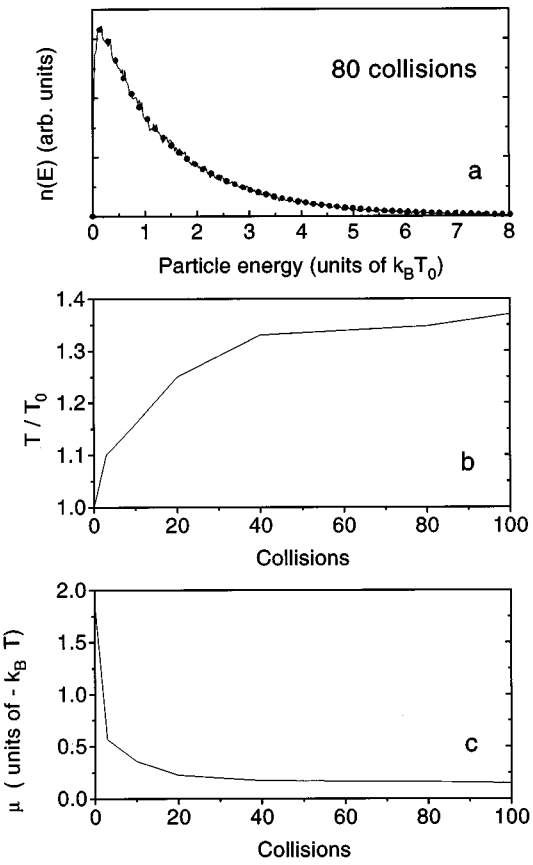

FIG. 1. In (a) particle energy distribution for a homogeneous sodium gas after 80 scattering events per particle; the dotted line is best fit by Bose-Einstein distribution of Eq. (21); in (b) temperature T from the best fits of the Bose-Einstein distribution vs scattering events; (c) the normalized chemical potential from the best fits vs scattering events. Initial values $T_0=2$ μK and $n_0=1.5\times10^{14}$ cm^{-3}.

where E is the single-particle energy, μ is the chemical potential, T is the temperature, $\epsilon=E/k_BT$, and $\alpha=-\mu/k_BT$. The use of this distribution function requires the validity of sufficient ergodicity, i.e., that the phase-space distribution of particles is only a function of the single-particle energy E. Note that this hypothesis of ergodicity is not being introduced into our numerical simulation, and that the fit of the particle energy distribution by Eq. (21) allows us to verify the validity of ergodicity assumption during the time evolution of evaporation.

When fitting the particle energy distribution, we multiply Eq. (21) by the density of states which is proportional to $E^{1/2}$ for constant potential energy and proportional to E^2 for a harmonic potential. By using Eq. (21) to fit the particle energy distribution, we can get the chemical potential and the temperature of the Bose gas, as shown in Figs. 2(b) and 2(c). For a homogeneous Bose gas, the total number of bosons N and the total energy U are given by [31,37]

$$N=V\left(\frac{2\pi M}{h^2}\right)^{3/2}(k_BT)^{3/2}\int f(\epsilon,\alpha)\epsilon^{1/2}d\epsilon+N_0,$$

$$U=V\left(\frac{2\pi M}{h^2}\right)^{3/2}(k_BT)^{5/2}\int f(\epsilon,\alpha)\epsilon^{3/2}d\epsilon, \qquad (22)$$

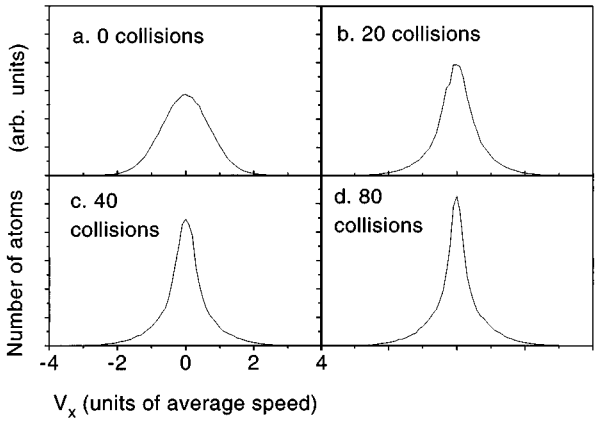

FIG. 2. The dynamical evolution of velocity distribution along x (or y,z) direction after different scattering events for the same conditions as in Fig. 1. The narrow peak at the central part indicates the accumulation of bosons at low-energy states and the short Gaussian background accommodates the usual thermal particles.

where V is the volume of the gas, h is the Planck's constant, and N_0 is the population at zero kinetic energy (for spin-polarized atomic gases the degeneracy factor is unity). For a system with constant energy, the mean energy E per particle, initially equal to $3k_BT_0/2$, is thus

$$\overline{E}=U/N=(k_BT)G(\alpha). \qquad (23)$$

For a classical gas where the normalized chemical potential α is much larger than 1, the function $G(\alpha)$ has the well-known value of 3/2 and decreases to zero as α decreases.

Our results for the homogeneous gas are in reasonable agreement with a previous work [31], however, since we consider the momentum and position of each boson instead of their energy, we can observe the evolution of velocity distribution which has been taken as one aspect for diagnosing the presence of the Bose-Einstein condensate experimentally [5,6]. In Fig. 2 the dynamical evolution of the velocity distribution is shown. It is found that after about 20 scattering events, the velocity distribution deviates from the Gaussian obviously, but the gas is still quite far from the equilibrium state. It is interesting to note that the velocity distribution after several more scatterings in Fig. 2 can be decomposed into two components: the central narrow peak for the low-energy Bose particles and the Gaussian for the background thermal particles. The observation of the non-Gaussian velocity distribution indicates the accumulation of Bose particles at low-energy states, but it is not necessarily the signature of the appearance of a macroscopic Bose-Einstein condensate.

B. Inhomogeneous gas in a harmonic potential at a fixed value

We now consider an ensemble of sodium atoms magnetically trapped in a harmonic potential. In the simulation the oscillation frequencies of the harmonic oscillator $(\omega_x,\omega_y,\omega_z)$ along three spatial directions are $(300,400,800)\times2\pi$ rad s^{-1}. The initial temperature T_0 of the gas is 2μK, the initial elastic collision rate 100 s^{-1}, and the elastic collision cross section 6×10^{-12} cm^2. The central

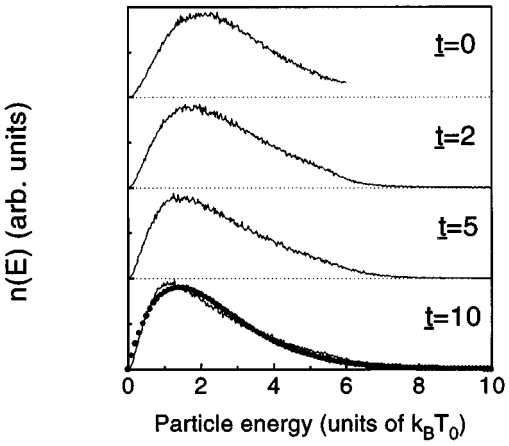

FIG. 3. The particle energy distribution for an inhomogeneous sodium gas at a fixed harmonic potential truncated for natural evaporation at $6k_BT_0$. The big dotted line shows the best fit by Eq. (21). Initial temperature is $T_0=2\ \mu$K with 1.54×10^6 Bosons and with a peak density of 3×10^{14} cm^{-3}. The natural evaporation is performed in three-dimensional position space. In this and following figure captions, dimensionless time $\underline{t}=t/\tau_i$ is used.

density n_0 is two times the critical density n_c for the Bose condensation at temperature T_0, where $n_c=1.5\times10^{14}$ cm^{-3}. The parameters above and the harmonic potential model are close to those used in the sodium experiments to observe Bose-Einstein condensation in Refs. [6,38].

We first consider the case when the threshold is fixed at a truncated value of $6k_BT_0$—the atoms whose potential energy is above this threshold are assumed to be lost during evaporation, and we call this fixed-threshold evaporation to distinguish it from forced evaporative cooling (the initial distribution is a Maxwell-Boltzmann distribution truncated at $6k_BT_0$). For the system we are considering, the quantum energy level spacing is much less than the thermal energy k_BT, so the system can be described by a continuum of states plus the ground state which has the zero-point energy [39]. The condensate fraction is defined as the population whose energy is within the lowest-energy bin, with size of 1/100 times k_BT_0. In Fig. 3 we show the evolution of the energy distribution in this case. Even though the initial total energy is truncated at $6k_BT_0$, higher-energy particles are produced because of interatomic collisions and the natural evaporative loss of atoms is based on the potential energy of atoms being above the threshold model. In this case the equipartition theorem between kinetic energy and potential energy is not strictly valid. This leads to a difference between the simulation results of the three-dimensional position cut model and the energy cut model in later sections. One can also note the particle flux towards the low-energy regime. By using the Bose-Einstein function of Eq. (21) to fit the particle energy distribution, as shown by the dotted line in Fig. 3, we get the chemical potential and the temperature of the Bose gas. The fit is not particularly good—we attribute the difference either to the fact that the gas is quite far away from equilibrium state or to the fact that the hypothesis of ergodicity required for the application of Eq. (21) is not valid. An important difference from the homogeneous gas is that the temperature of the Bose gas decreases as scattering proceeds, since hot

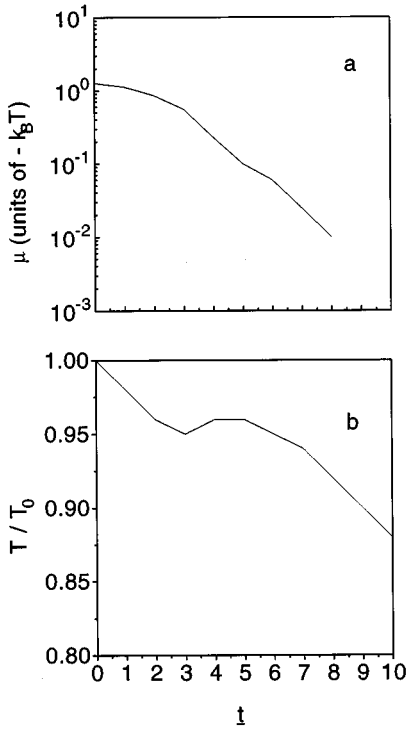

FIG. 4. In (a) normalized chemical potential and in (b) temperature, as derived from the best fits using Eq. (21), vs time, in dimensionless units, for an inhomogeneous gas at a fixed harmonic potential as in Fig. 3. At $\underline{t}=8$, the fit error of the chemical potential is comparable to its absolute value so no further value is shown.

atoms are allowed to escape from the trap, as shown in Fig. 4(b). The production of high-energy Bose particles by elastic scattering is further aided by the $1+f(\mathbf{k_i})$ factor. Due to the decrease of the temperature, the chemical potential approaches to zero quickly, as shown in Fig. 4(b) (at $t=8\tau_i$, the fit error of the chemical potential is quite large compared to its absolute value, so no further values are shown) [40]. In Fig. 5 the condensate fraction is shown. It can be seen that the condensate fraction is very small and it increases linearly with time—we did not observe a sudden increase in condensate population. Even for times as long as $200\tau_i$ (not shown) an equilibrium state has not been reached, although the mean

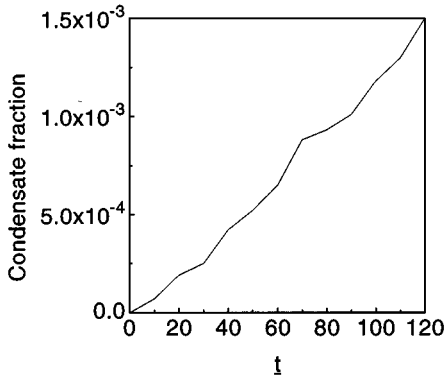

FIG. 5. The condensate fraction vs time at a fixed harmonic potential truncated at $6k_BT_0$ with the same initial conditions as in Fig. 3.

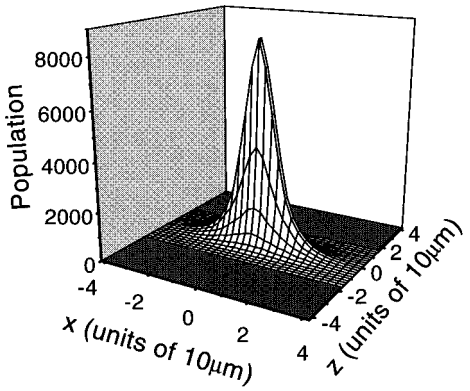

FIG. 6. The spatial distribution at time $t=120$ with a fixed harmonic potential truncated at $6k_BT_0$ with the same initial conditions as in Fig. 3.

collision rate increases by a factor of 6. In the simulations of Fig. 4 the mean energy decreases from 1.82 μK to 0.76 μK [42], and the total number of bosons drops from 1.54×10^6 to 1.13×10^6. Once again the velocity distribution becomes non-Gaussian, as in Fig. 2, after about 20 scattering events per particle in average (at $t=12\tau_i$), but the condensate fraction is very small, as shown in Fig. 5. The position distribution at $t=120\tau_i$ is shown in Fig. 6, where the distribution is anisotropic due to the difference between oscillation frequencies along x and z. The central peak at $z=0$ deviates from Gaussian. This nonclassical spatial distribution is similar to that obtained by Plimak and Walls [43].

C. Inhomogeneous gas in presence of forced evaporation

From the results in Sec. III B it is clear that it is quite difficult to put most of the bosons into a quantum degenerate regime only by Bose scattering and natural evaporation. So in order to speed up kinetic evolution of the Bose gas, forced evaporative cooling has to be applied. To initiate forced evaporative cooling, we take the final phase-space distribution function after natural evaporation at $t=120\tau_i$ as the initial distribution function. The initial mean energy is 0.83 μK with 1.15×10^6 bosons. The cutoff energy $E_{\rm cut}(t=0)$ initially $6k_BT_0$, as in natural evaporation, in forced evaporation is ramped downwards exponentially. We consider four models for evaporative cooling. The first one assumes that the bosons are removed in terms of the single-particle energy [8–10], i.e., the bosons are assumed to be lost when the following relation is valid:

$$\sum_{i=x,y,z}\frac{1}{2}M\omega_i^2x_i^2+\frac{1}{2}Mv_i^2>E_{\rm cut}(t)=E_{\rm cut}(0)e^{-t\times\ln2/15\tau_i}. \tag{24}$$

The other three cuts consider the particle's position or its potential energy. They are three-, two-, and one-dimensional evaporation, respectively, corresponding to three equations for cutting, $\sqrt{x^2+(y\omega_y/\omega_x)^2+(z\omega_z/\omega_x)^2}\geqslant r_{\rm initial}\times e^{-t\times\ln2/30\tau_i}$, $\sqrt{x^2+(y\omega_y/\omega_x)^2}\geqslant r_{\rm initial}e^{-t\times\ln2/30\tau_i}$, and $x\geqslant r_{\rm initial}\times e^{-t\times\ln2/30\tau_i}$, respectively, with $r_{\rm initial}=50$ μm. In all cases the forced evaporation is performed in 60 τ_i and, in total, the trap depth is decreased by a factor of 16. After forced evaporation is stopped we let the gas evolve for another $20\tau_i$ in order to equilibrate different degrees of freedom. It is generally thought that the two-dimensional evaporative cooling model is close to the case in a TOP (time-averaged orbiting potential) magnetic trap [5,12], since in a TOP trap atoms are mainly removed in terms of their radial positions. On the other hand, the unfavorable oscillation of the center of mass of the atomic cloud, which can be caused by the initial displacement from the bottom of the potential when one loads an atomic cloud from a magneto-optical trap into a TOP trap, and the gravity can easily make the forced evaporation be two- or even one-dimensional [44,45] in practice. At present it is not clear which evaporation model represents the real process in an experiment and the question needs to be addressed by making a detailed comparison between theory and experiments.

Figure 7 shows the simulation results. It can be seen the higher the dimension of the cuts (an energy cut can be thought as six-dimensional evaporative cooling), the higher the efficiency. In Fig. 7(a) we did not observe the cross over for two- and three-dimensional evaporation, as in the classical simulation [11], even when evaporation is deeper and quicker. Figure 7(b) indicates the macroscopic condensate fraction at ground state and the formation of quantum degeneracy in this level—the sharp increase of the condensate is also visible. Figure 7(c) shows the decrease of the mean energy by a factor around 8, and Fig. 7(d) indicates evolution of the particle energy distribution for three-dimensional evaporation. Evaporative cooling is based on the removal of energetic particles whose production is enhanced by Bose scattering properties. Comparing Fig. 7(b) with Fig. 5 one can note that forced evaporation plays an important role in putting Bosons into the quantum degenerate regime. In Fig. 7 after evaporation stopped, we let the Bose gas evolve for further 20 initial collision times while the energy cut remained at the final value, except for one case denoted by the big dotted line. This situation of a fixed final energy cut corresponds closely to what is actually done during the formation of the Bose-Einstein condensate in the experiments and seems to produce a higher condensed fraction. The big dotted line in Fig. 7 indicates the case for two-dimensional evaporative cooling when the cut energy returns to the initial value of $6k_BT_0$ after evaporation stopped. This would approximately correspond experimentally to the case of the evaporation process being switched off while the system equilibrates [5,38]. In this case the total number of bosons remains unchanged, as shown by the big dotted line in Fig. 7(a), the mean energy has a weak increase, as shown in Fig. 7(b). However, the condensed fraction is less, and the absolute condensate population is also reduced. For the cases of the cut remaining at its final value or returning to its initial value, the condensate population is 1.25×10^5 and 5.92×10^4, respectively.

Figure 8 shows the lag between the axial and the radial mean energies in two-dimensional evaporation. Even though it is quite surprising that even at time $t=20\tau_i$, i.e., after 20 initial collision times, one can still notice some difference between the radial and axial energies, it seems to be consistent with the experimental observation [46]. We have also

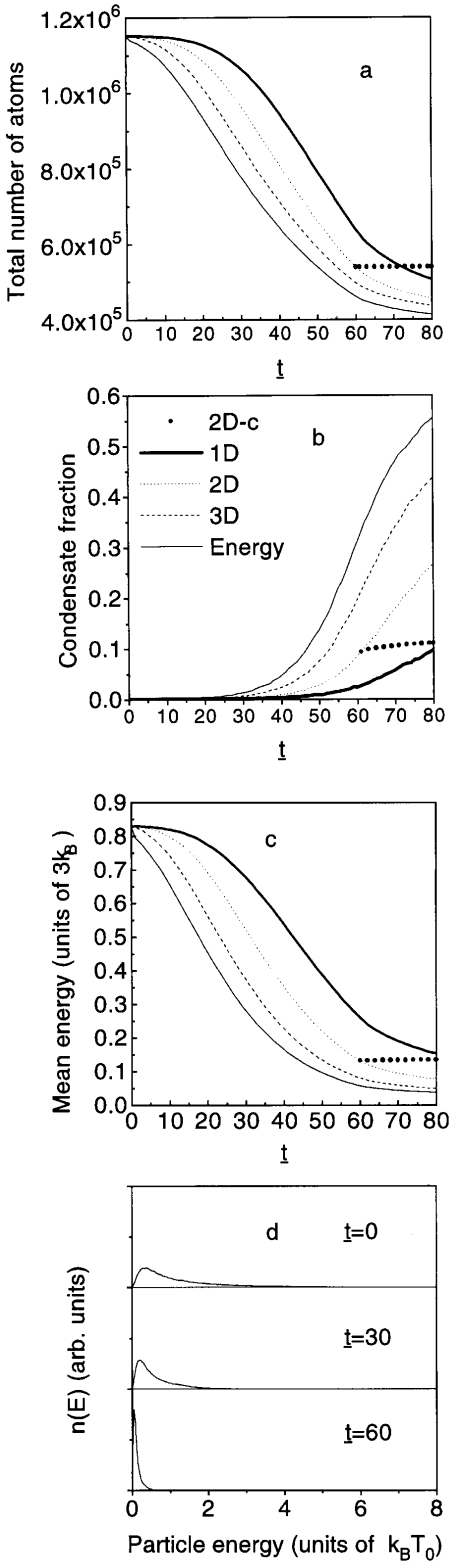

FIG. 7. In (a) the number of particles; in (b) the condensate fraction; in (c) the mean energy vs time for forced evaporative cooling. The trap depth decreases exponentially by a factor of 16 in a time of $60\tau_i$. Forced evaporation stops at $\underline{t}=60$, the gas is allowed to evolve for another 20 initial collision times. Except the big dotted line [2D in (c)], where the cut returns to initial trap depth of $6k_BT_0$, in other cases the cut remains fixed at the value where it was stopped. In (d) particle distribution for three-dimensional forced evaporative cooling.

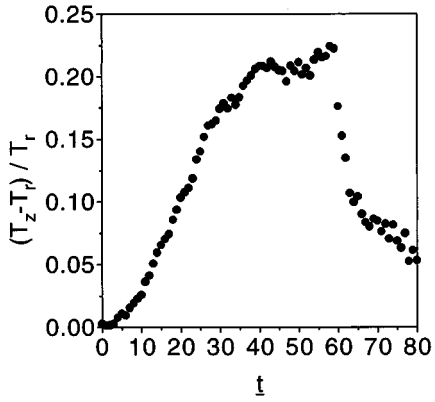

FIG. 8. The lag between the mean axial energy T_z and radial energy $T_r=(T_x+T_y)/2$ for two-dimensional forced evaporative cooling. After forced evaporation stops at $\underline{t}=60$, the cut energy returns to $6k_BT_0$.

observed the lag between the axial and the radial mean energies for the case of one-dimensional evaporation.

D. Comparison with classical trajectory method

There have been four papers on evaporative cooling published in the last year [8–11], all of which use quite different methods of calculation. Our simulation uses Bird's method as described in previous sections. All other ones consider energy evolution. All four methods consider $\lambda_{dB}\gg R_0$, where $\lambda_{dB}=[2\pi\hbar^2/(mk_BT)]^{1/2}$ is the thermal de Broglie wavelength and R_0 is the range of the interatomic potential. For this case, the quantum-mechanical scattering is solely s-wave scattering. In this section we make a comparison with other methods, in particular, with the classical trajectory method [10]. In order to make this comparison, we did not consider the quantum statistics effect, or the $1+f(\mathbf{k_i})$ factor in the scattering matrix of Eq. (20), and we had to work with an energy cutoff rather than a position dependent cutting.

The first method, developed by Davis, Mewes, and Ketterle [8], assumes that the atomic energy distribution can always be described by a truncated Maxwell-Boltzmann distribution and calculates the final state after the gas has recovered thermal equilibrium [1,2,8]. This simple method qualitatively tells one how the forced evaporative cooling works. One important result of this work is that the threshold density for accelerated evaporation is higher in a parabolic trap than in a spherical quadrupole (three-dimensional linear) trap, and the increase in the collision rate in a harmonic potential is small, and only occurs for appropriate cuts in the potential well. In our simulation where a three-dimensional harmonic potential is used, the small increase in the collision rate is observed when a three-dimensional cut is performed [11], which is consistent with their conclusions.

Luiten, Reynolds, and Walraven [9] considered the nonequilibrium process of evaporation by solving the Boltzmann equation, however, because it is extremely difficult to solve this nonlinear six-dimensional equation directly, they introduced the assumption of sufficient ergodicity [9,31,33]. One important result of that work is that the phase-space distribution of atoms in a trap can often be described by a truncated Maxwell-Boltzmann distribution.

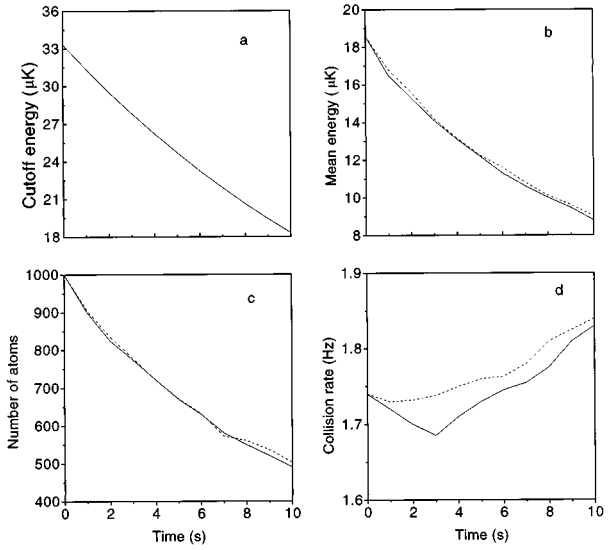

FIG. 9. Comparison of our calculations using Bird's method (solid line) and the results of classical trajectory method of Holland *et al.* [10] (dashed line). (a) Cut energy divided by $3k_B$ used in these two methods; (b) the calculated mean energy of the distribution divided by $3k_B$; (c) number of atoms remaining in the trap; (d) collision rate of atoms. The difference between the two methods arises from statistical fluctuations.

Even though the ergodic assumption simplifies the Boltzmann equation significantly, numerically there are still some difficulties because of its nonlinearity. Therefore, a classical trajectory method (alluding to its similarity with the quantum trajectory method) was developed by Holland *et al.* [10]. This approach also assumes sufficient ergodicity, with a computation time linearly proportional to the number of points used to sample the distribution function. We have made a detailed comparison with this classical trajectory method to verify our calculations. The physical parameters used in Ref. [10] are collision cross section $\sigma=10^{-8}$ m^2, mass $M=2.26\times10^{-25}$ kg, angular oscillation frequencies $(\omega_x,\omega_y,\omega_z)=(9,16,18)$ rad s^{-1} (i.e., numbers include factor 2π), $T_{\text{initial}}=25$ μK. The cut energy decreases as $E_{\text{cut}}=E_{\text{cut}}(0)e^{-\kappa t}$, which is illustrated in Fig. 9(a), where $E_{\text{cut}}(0)/3k_B=33$ μK and cut rate constant $\kappa=0.06$ s^{-1}, the initial mean energy of the atomic cloud being 18.6 μK for the truncated Maxwell-Boltzmann distribution [42]. The number of atoms within the initial truncated distribution is $N_0=1000$. Use of small trap oscillation frequencies makes calculation quicker since larger time steps can be used. The evolution was simulated for 10 s.

In Fig. 9 we show the simulation results for these two methods, where the solid line is for Bird's method and the dashed line is for the trajectory method taken from [10]. It can be seen that these two methods are consistent. The difference in the collision rates in Fig. 9(d) arises from the statistical noise in the simulations (the total increase of collision rates is only around 5%, and the fluctuation is around 1%, it may take large number of simulations to get rid of this statistical noise). In both approaches, a tiny increase of the collision rate is observed. This means that, in the case of the energy cut, it is possible to reach runaway evaporation.

IV. CONCLUSION

By using molecular gas dynamics we have simulated forced evaporative cooling incorporating quantum statistics, while all the simulations published before were purely classical [8–11]. Our powerful approach does not need the common assumption of sufficient ergodicity or quasiequilibrium during forced evaporation as other methods. Therefore, it allows us to study rapid forced evaporative cooling far from the equilibrium state in one-, two-, and three-dimensional position cuts. In the simulations of one- and two-dimensional cuts, it was found that when the cut was stopped there was a difference in energy between axial and radial directions. We have also studied the dynamical formation of the Bose-Einstein condensate in homogeneous and inhomogeneous gases considering quantum statistics under the random-phase approximation. It was found that it takes quite a long time to reach an equilibrium state for both homogeneous and inhomogeneous gases. The dynamical evolution from a noncondensed system to a Bose condensate is purely a nonequilibrium process. For a homogeneous Bose gas the temperature increases as the formation of quantum degeneracy due to energy conservation, while it decreases for an inhomogeneous gas in a finite potential due to evaporation. The observation of the non-Gaussian velocity distribution indicates the accumulation of low-energy Bose particles but does not necessarily indicate the formation of a macroscopic population at ground state. For an inhomogeneous gas in a potential, the Bose scattering process, which puts bosons into the ground state, is further aided by forced evaporation and a macroscopic population accumulation at ground level can be reached, which is consistent with experimental results. In our simulations we have assumed an initial density large enough to produce a runaway evaporative cooling. The present approach could be also applied to investigate the evolution of clouds of cold atoms with an initial atomic density lower than the value required for runaway evaporation, with the spring constant of the harmonic potential ramped up to increase the atomic density.

In the future it will be very interesting to make a comparison between our present results and that obtained using the quantum kinetic master equation [36]. This equation preserves the full quantum-mechanical description of the condensate and considers the modification of the noncondensate spectrum by the condensate by separating coherent processes from scattering processes. Moreover, hopefully, our calculations will be compared to experimental measurements to test whether the cutting is effective only in the radial direction (two dimensional) in a TOP trap, and whether the gravity effect can effectively make the evaporation two- or even one-dimensional.

ACKNOWLEDGMENTS

We are indebted to K. Burnett, E. Cornell, J. Dalibard, S. Giorgini, and M. Holland for very helpful discussions. H.W. acknowledges support within the European Community Network on Atom Optics. We thank Professor F. Bassani and the Computer Center of the Scuola Normale Superiore for allowing us to have access to computer facilities.

[1] H. F. Hess, Phys. Rev. B **34**, 3476 (1986).
[2] N. Masuhara, J. M. Doyle, J. C. Sandberg, D. Kleppner, and T. J. Greytak, Phys. Rev. Lett. **61**, 935 (1988).
[3] W. Petrich, M. H. Anderson, J. R. Ensher, and E. A. Cornell, Phys. Rev. Lett. **74**, 3352 (1995).
[4] K. B. Davis, M. O. Mewes, M. A. Joffe, M. R. Andrews, and W. Ketterle, Phys. Rev. Lett. **74**, 5202 (1995).
[5] M. H. Anderson, J. R. Ensher, M. R. Matthews, C. E. Wieman, and E. A. Cornell, Science **26**, 198 (1995).
[6] K. B. Davis, M. O. Mewes, M. R. Andrews, N. J. van Druten, D. S. Durfee, D. M. Kurn, and W. Ketterle, Phys. Rev. Lett. **75**, 3969 (1995).
[7] C. C. Bradley, C. A. Sackett, J. J. Tollett, and R. H. Hulet, Phys. Rev. Lett. **75**, 1687 (1995).
[8] K. B. Davis, M. O. Mewes, and W. Ketterle, Appl. Phys. B **60**, 155 (1995).
[9] O. J. Luiten, M. W. Reynolds, and J. T. M. Walraven, Phys. Rev. A **53**, 381 (1996); see also O. J. Luiten, Ph.D. thesis, University of Amsterdam, 1993.
[10] M. Holland, J. Willams, K. Coakley, and J. Cooper, Quantum Semiclassic. Opt. **8**, 571 (1996).
[11] H. Wu and C. J. Foot, J. Phys. B **29**, L321 (1996).
[12] W. Ketterle and N. J. van Druten, in *Advances in Atomic, Molecular and Optical Physics*, edited by B. Bederson and H. Walther (Academic, San Diego, in press), Vol. 37, p. 181.
[13] E. L. Surkov, J. T. M. Walraven, and G. V. Shlyapnikov, Phys. Rev. A **53**, 3403 (1996); J. T. M. Walraven, in *Quantum Dynamics of Simple Systems*, edited by G. L. Oppo, S. M. Barnett, E. Riis, and W. Wilkinson (IOP, Bristol, 1996), p. 316.
[14] G. A. Bird, *Molecular Gas Dynamics and the Direct Simulation of Gas Flow* (Clarendon, Oxford, 1994).
[15] A. Martin, K. Helmerson, V. S. Bagnato, G. P. Lafyatis, and D. E. Pritchard, Phys. Rev. Lett. **61**, 2431 (1988); K. Helmerson, A. Martin, and D. E. Pritchard, J. Opt. Soc. Am. B **9**, 1988 (1992).
[16] C. R. Monroe, E. A. Cornell, C. A. Sackett, C. J. Myatt, and C. E. Wieman, Phys. Rev. Lett. **70**, 414 (1993).
[17] H. Wu, P. Xu, and W. Luo, J. Phys. D **26**, 1351 (1993).
[18] H. K. Chen and G. Emanuel, AIAA J. J. **33**, 385 (1995).
[19] I. Choquet, Phys. Fluids **6**, 4042 (1994).
[20] T. Kunugi and H. Yasuda, Fusion Eng. Des. **28**, 162 (1995).
[21] K. Sugiyama, H. Yoshida, and R. Ishiguro, J. At. Eng. Soc. Jpn. **36**, 976 (1994).
[22] C. R. Justiz, R. M. Sega, and C. Dalton, J. Comput. Phys. **118**, 278 (1995).
[23] A. V. Vasenkov, A. E. Belikov, R. G. Sharafutdinov, and O. V. Kuznetsov, J. Appl. Phys. **77**, 4757 (1995).
[24] A. L. Garcia, F. Baras, and M. M. Mansour, Phys. Rev. E **51**, 3784 (1995).
[25] E. Klein and Y. Stephan, in *Monte-Carlo Methods, Lecture Notes in Physics*, edited by R. Alcouffe *et al.* (Springer, Berlin, 1985), p. 454.
[26] D. Soubbaramayer (unpublished).
[27] H. Wu (unpublished).
[28] W. H. Press, B. P. Flannery, S. A. Teukolsky, and W. T. Vetterling, *Numerical Recipes* (Cambridge University, Cambridge, England, 1988).
[29] H. Wu, M. J. Holland, and C. J. Foot, J. Phys. B **28**, 5025 (1995).
[30] S. Chapman and T. G. Cowling, *The Mathematical Theory of Non-uniform Gases* (Cambridge University, Cambridge, England, 1970).
[31] D. W. Snoke and J. P. Wolfe, Phys. Rev. B **39**, 4030 (1989).
[32] Yu Kagan, in *Bose-Einstein Condensation*, edited by A. Griffin, D. W. Snoke, and S. Stringari (Cambridge University, Cambridge, England, 1995), p. 202.
[33] Yu Kagan, B. V. Svistunov, and G. V. Shlyapnikov, Zh. Eksp. Teor. Fiz. **101**, 528 (1992) [Sov. Phys. JETP **75**, 387 (1992)].
[34] H. T. C. Stoff, in *Bose-Einstein Condensation*, edited by A. Griffin, D. W. Snoke, and S. Stringari (Cambridge University, Cambridge, England, 1995), p. 226.
[35] E. Levich and V. Yakhot, Phys. Rev. B **15**, 243 (1977).
[36] C. W. Gardiner and P. Zoller (unpublished).
[37] P. M. Morse, *Thermal Physics* (Benjamin, New York, 1964), p. 346.
[38] M.-O Mewes, M. R. Andrews, N. J. van Druten, D. M. Kurn, D. S. Durfee, and W. Ketterle, Phys. Rev. Lett. **77**, 416 (1996).
[39] V. Bagnato, D. E. Pritchard, and D. Kleppner, Phys. Rev. A **35**, 4354 (1987).
[40] The density of states inside the harmonic potential is modified by the interaction between the atoms, as calculated in the mean potential approach. This modification of the density of states has an influence on their occupation, so that the chemical potential rises above its value of zero-point energy, and becomes a function of the number of atoms in the system. In our simulation the chemical potential, initially negative, approaches zero with the accumulation of low-energy particles, while it is positive for a Bose gas with a positive scattering length in a trap when interaction energy is included [41].
[41] G. Baym and C. J. Pethick, Phys. Rev. Lett. **76**, 6 (1996).
[42] To describe a truncated Maxwell-Boltzmann distribution, the temperature is not the most appropriate parameter. Thus we specify such a distribution by its mean energy, which results in smaller than k_B times the temperature of the nontruncated original distribution.
[43] L. I. Plimak and D. F. Walls, Phys. Rev. A **54**, 652 (1996).
[44] W. Ketterle (unpublished).
[45] A. Wilson, J. Martin, P. Bance, and C. J. Foot (unpublished).
[46] E. Cornell (private communication).